Mechanisms of Oscillatory Reactions Deduced from Bifurcation Diagrams

Igor Schreiber[†] **and John Ross***[,‡]

Department of Chemistry, Stanford University, Stanford, California 94305, and Department of Chemical Engineering, Prague Institute of Chemical Technology, 166 28 Prague 6, Czech Republic

Received: May 13, 2003; In Final Form: September 3, 2003

The classification/categorization of oscillatory chemical reactions and the determination of the connectivity of species in a reaction mechanism can be deduced from several experiments. In this article we show the same for bifurcation diagrams. We construct such diagrams for skeletal models of each of the known categories; these are distinct and can be used for the classification of species essential for oscillations and for the categorization of oscillatory reactions. The bifurcation diagrams are closely related to the concentration shift matrix. Prototypes of categories 1B and 1C are extended by adding nonessential species. By assuming that in a flow-through stirred reactor bifurcation diagrams for each pair of constraints (the inflow concentrations and the flow rate) can be measured, we are able to determine the category of the examined oscillator and also deduce the connectivity of the corresponding reaction network. Bifurcation diagrams possess a cusp region with specific tilt. This information together with the knowledge of a concentration shift across the saddle-node bifurcation provide the clues for categorization as well as for the reconstruction of the network's connectivity. As an example, we present an analysis of the Belousov−Zhabotinsky reaction represented by the Field−Körös−Noyes mechanism and discuss the feasibility of reconstruction of the mechanism from experiments.

1. Introduction

Mechanisms of reaction systems with oscillatory dynamics or multiple stationary states can be categorized according to basic features in their reaction networks,[1] such as autocatalytic loops, exit reactions, and negative feedback loops. This categorization is based in part on stoichiometric network analysis (SNA),[2] which provides a convenient tool of decomposing the entire network operating at a stationary state into subnetworks and indicates those which can cause the network's stationary state to become unstable. Defining *categories for oscillatory mechanisms* also implies a *classification of species* taking part in those mechanisms. In Eiswirth et al.[1] and in subsequent work,[3−9] several experiments for classifying species and determining the reaction categories were proposed and tested on the chlorite−iodide reaction and horseradish peroxidase reaction. Moreover, these experiments help to deduce rather than guess the connectivity of the reaction network and other features that are useful for identification of the reaction mechanism. Among those experiments are the following:[4] (I) amplitude and phase relation of oscillations of chemical species, (II) concentration shift regulation and destabilization, (III) pulsed species response, (IV) phase response, (V) Jacobian matrix elements, (VI) quenching, and (VII) bifurcation analysis.

For these and yet other experiments the relation of the experimental results to information about the reaction mechanism has been worked out fully except for items IV, V, and VII.

Hence we focus here on using bifurcation diagrams determined from experiments for the categorization and deduction of the connectivity of the network. The use of bifurcation diagrams for categorization has been initiated in ref 1; here we follow those studies to establish complete relations, particularly to concentration shift experiments, and hence to categorization. There have been several attempts to use bifurcation diagrams to decide between proposed alternative mechanisms. Noszticius et al.[10] studied the Belousov−Zhabotinsky (BZ) reaction in a flow-through reactor with various chemical reagents being fed in and concluded that the bifurcation diagrams can be used as fingerprints of the perturbing reagent. Olsen and Epstein[11] examined the effect of alternative proposed pathways on calculated bifurcation diagrams, compared them with available experiments, and suggested further experiments for the mixed Landolt and chlorite−iodide reactions. Ringland[12] showed how certain codimension 2 points in a bifurcation diagram for a seven-variable model of the BZ reaction can be used to accept/exclude the model when compared with experimental data.

By means of several examples we show how the task of mechanism determination may be systematically approached using the bifurcation diagrams (and closely related concentration shift matrices) constructed from experiments in a flow-through reactor, where the flow rate and inflow concentration of each species is systematically varied to provide two-parameter bifurcation diagrams. These diagrams typically contain a cusp-shaped region of multiple stationary states and essentially delineate regions of oscillatory and nonoscillatory behavior, as well as regions of bistability between stationary states. A predominantly occurring structure called the *cross-shaped diagram*[13] involves the cusp-shaped region bounded by a curve corresponding to a saddle-node bifurcation, and a curve corresponding to a Hopf bifurcation that makes an α-shaped loop surrounding the cusp point, intersects itself within the cusp-shaped region, and touches the saddle-node curve in two points of codimension 2 (Bogdanov−Takens points). Thus the oscil-

* Address correspondence to this author. E-mail: john.ross@stanford.edu. Fax: 650 723 4817.
[†] Prague Institute of Chemical Technology.
[‡] Stanford University.

10.1021/jp035310t CCC: $25.00
Published on Web 10/28/2003

latory region extends beyond the tip of the cusp; bistability is confined to the interior of the cusp and excitability occurs in between. This highly symmetric structure may not always be present; in many cases the self-intersection is missing or there are two separate branches of the Hopf bifurcation.

Nevertheless, the primary feature is the tilt of the cusp-shaped region; the actual arrangement of the oscillatory region is secondary in the mechanism determination. Along with the bifurcation diagrams, one-parameter diagrams of stationary state concentrations near the cusp are useful in providing information about the mechanism. We discuss how these two types of diagrams can be used to determine the category, to classify the species, and how to tie the essential and nonessential species to the reaction network.

In Section 2 we construct representative bifurcation diagrams for skeletal models of each of the known categories of chemical oscillators. Each category has its own distinctive bifurcation diagrams, and hence these can be used for the classification of essential species and for categorization of the reactions.

In Section 3 we show that the bifurcation diagrams are closely related to the concentration shift matrix; then we construct a global concentration shift matrix and formulate rules for this matrix which can be used in the reverse problem, that of a systematic reconstruction of a reaction network. As a preliminary example of the reconstruction procedure we extend prototypes of categories 1B and 1C by adding nonessential species, calculate bifurcation diagrams, transform them to the global shift matrix, and then describe the reconstruction of the network.

In Section 4 we apply these results to the problem of deducing a network's connectivity from experimentally obtained bifurcation diagrams. We calculate bifurcation diagrams for the FKN mechanism[14,15] of the BZ reaction and discuss the reconstruction of the mechanism based on these diagrams. Then we discuss the experimental feasibility of such a reconstruction. We have also investigated successfully the mixed-Landolt (iodate−sulfite−ferrocyanide) reaction,[16−18] but the preliminary results are not presented here.

Appendices A and B contain necessary elements of the SNA theory and basic facts from the classification and categorization of oscillatory mechanisms.

2. Calculations of Bifurcation Diagrams of the Categories of Oscillatory Reactions

Oscillatory reactions can be grouped into several distinct categories based on the aforementioned experiments. Since the categorization process makes use of SNA,[2] necessary elements of that theory are reviewed in Appendix A; the fundamentals of classification/categorization established in previous work[1,3,4,9] are given in Appendix B. We also refer the reader to both Appendices for the notation and basic form of equations assumed throughout.

Once the classification/categorization is established one can proceed to obtain more detailed information about the unknown parts of the mechanism by deducing their network connectivity (particularly with respect to nonessential species) from experiments of type III and IV as described earlier[4,8] and also from experiments of type II and VII as will be shown here.

To develop the categorization derived from bifurcation diagrams we begin with the use of SNA to locate an organizing point capturing the oscillatory and multiple stationary state dynamics, and from there we proceed with construction of the bifurcation diagrams representing each category.

2.1. Bifurcation Diagrams in SNA Parameters. Categorization relies on typical features shared by a group of mutually related networks. Therefore paradigmatic examples provided for each category in prior work[1−9] need not be examined for every possible combination of parameters; rather, a point or region in the parameter space reflecting typical behavior may be selected to demonstrate categorization criteria. Since we are examining systems displaying in general either oscillatory dynamics or multiple stationary states we first search for an organizing singularity that involves both features. Such a situation is provided by a Bogdanov−Takens (BT) bifurcation associated with a double zero eigenvalue of the Jacobian at the stationary state; this is a codimension 2 bifurcation, where a saddle-node bifurcation (giving rise to multiplicity) and a Hopf bifurcation (giving rise to oscillations) meet. In two-parameter bifurcation diagrams this corresponds to a point where a Hopf bifurcation curve terminates and touches a saddle-node bifurcation curve. By starting with a BT point we can track the emanating bifurcation curves by numerical continuation methods[19] and construct the bifurcation diagram.

To select a BT point we employ a parametrization as used in SNA[2] (see Appendix A for more detail); instead of the reaction rate coefficients k_1, ···, k_r (internal parameters) and the flow rate k_0 and inflow concentrations x_{01}, ···, x_{0n} (external constraints) we turn to the coefficients α_k, used in expressing a general reaction rate vector (current) as a linear combination of specific rate vectors representing major reaction subnetworks (extreme currents), and the stationary state concentrations x_{s1}, ···, x_{sn} of the species involved. For a given network representing a given category, we first calculate from its stoichiometric matrix ν the set of extreme currents $\{e_k\}$. Then we examine their stability matrix V (see eq A4) and identify the potentially unstable ones. This is indicated by negative principle minors β of V. After that we choose stationary values of all concentrations so that their values for certain groups of l species (indicated by negative β_l) are small enough, so that the instability of the stationary state for the unstable e_k's is ensured. Next we combine all extreme currents by setting their α_k's so that a Hopf bifurcation point is obtained, taking into account certain constraints imposed by the flow-through arrangement. This task can be accomplished since we know the stability of the extreme currents from the previous steps; hence major positive and negative feedback loops can be identified and the corresponding currents combined to get an oscillatory instability. Finally, we select two extreme currents, one associated with oscillatory dynamics and the other one with multiplicity, and use the two corresponding α_k's as parameters to construct the Hopf bifurcation curve in a two-parameter bifurcation diagram and trace it down to the BT point.

We use the current evaluated at the BT point for switching from parametrization by α_k's (at fixed stationary state $x_s = (x_{01}, \cdots, x_{0n})$) to the usual parametrization by rate coefficients and external constraints. Since the values of reaction rates $v_1(x_s)$, ···, $v_r(x_s)$ in this current are known, as well as their functional form (power law kinetics are assumed), the reaction rate coefficients can be readily calculated. In this way, rather than being empirically chosen, the reaction rate coefficients are selected by design based on a dominance of certain key subnetworks in the linear combination of all extreme currents. This approach gives considerable insight into the way the basic subnetworks are put together to form the whole of the network.

2.2. Bifurcation Diagrams in External Constraints. The flow rate and inflow concentrations are the external constraints considered here. Eiswirth et al.[1] provide a table characterizing bifurcation diagrams of category 1 oscillators using various pairs of inflow concentrations X_0, Y_0, and Z_0 of the essential species

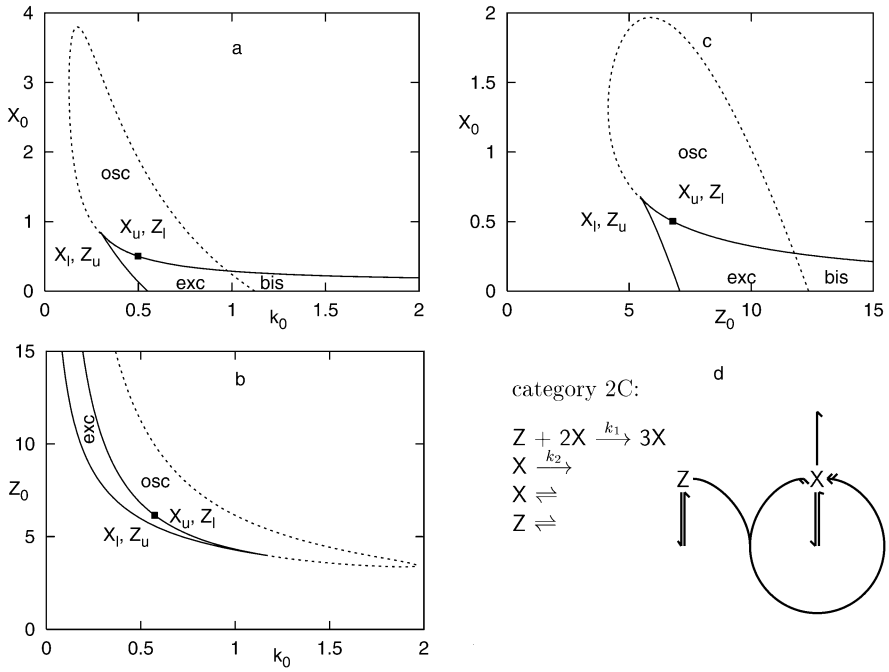

Figure 1. Bifurcation diagrams and reaction network for a prototype of category 2C. Rate coefficients used in calculations: $k_1 = 4.91569$, $k_2 = 5.04517$. Notation: solid line, saddle-node bifurcation; dashed line, Hopf bifurcation; square, BT point; osc, bis, exc, region of oscillations, bistable stationary states, and excitability, respectively. Fixed parameter values for the reference BT point: $k_0 = 0.5$, $X_0 = 0.5$, $Z_0 = 6.8$.

X, Y, and Z as bifurcation constraints. Following this approach we extend the table by using pairs of flow rate−inflow concentration, since they are frequently used in experimental studies. In all diagrams of this type the important feature is the orientation of the cusp with respect to the coordinate axes. Generically the cusp is tilted rather than being parallel to one of the coordinate axes. Consequently the "symmetry axis" of the cusp (the line to which both branches of the cusp curve are tangent at the tip) has generically either a positive or a negative slope; we call the two cases *diagonal* and *anti-diagonal*, respectively. Within each category the diagonal or anti-diagonal orientation is preserved for a given pair of constraints *regardless of the choice of rate coefficients*. Moreover, the tip of the cusp is directed specifically either to the left or to the right (with respect to the horizontal direction) for each essential species in each category. In addition, an oscillatory region may extend past the tip. *Therefore the pattern of the saddle-node and the Hopf curves can be used to indicate categories and classify essential species in much the same way as deductions from other experiments, such as the concentration shifts and phase shifts*.

Below we systematically construct and discuss bifurcation diagrams in external constraints for each category with emphasis on the flow rate−inflow concentration space.

2.2.1. Category 2C. The prototype for category 2C networks in Figure 1d (basically the Selkov model for glycolysis[20]) has two essential species of type X and Z; there are three constraints, the inflow concentrations X_0 and Z_0 and the flow rate k_0. The bifurcation diagrams for k_0-X_0, k_0-Z_0, and Z_0-X_0 are shown in Figure 1, parts a, b, and c, respectively. They all possess the same structure with an anti-diagonal cusp-shaped saddle-node bifurcation curve, and a Hopf bifurcation curve extending from a single BT point around the tip of the cusp. The cusp points up-left in parts a and c of Figure 1 and right-down in Figure 1b.

It is useful to distinguish two kinds of stationary states according to the relative level of the concentration of X or Z. Correspondingly, we label the concentration of each species at a stationary state that is not a saddle (but otherwise may be unstable) either as "upper" (X_u or Z_u) or "lower"' (X_l or Z_l). The two such stationary states in Figure 1 are (X_l, Z_u) and (X_u, Z_l); they coexist in the cusp region; the "lower" state with respect to the autocatalytic species X (and "upper" for Z) extends down-left from the cusp region—the autocatalytic pathway is unimportant under such conditions; the "upper" state for X (and "lower" for Z) extends up-right where the autocatalytic pathway dominates. As will be shown later, this labeling makes it possible to relate the bifurcation diagram to the concentration shift matrix.

Two main dynamical modes, oscillations (predominantly occurring within a region marked by a Hopf bifurcation), and bistable stationary states are labeled by osc and bis, respectively. However, bistability does not fill up the cusp region entirely because the Hopf bifurcation may destabilize one of the stationary states. In this case the remaining stable stationary state is excitable and we label the corresponding part of the cusp region by exc. The border between oscillatory and excitable regions is formed largely by a saddle-node-infinite-period (SNIPER) bifurcation where the threshold for excitability becomes zero.

Some features of the diagrams in Figure 1 are as follows:

(a) When Z_0 is small, Figure 1b,c, there is a unique stationary state while for large enough Z_0 regions of multiple stationary states and/or oscillations occur due to autocatalytic instability.

(b) The effect of X_0 is just the opposite. For arbitrarily small X_0 a region of multiplicity can always be found; at medium values of X_0 an oscillatory region exists while for large enough X_0 the stabilizing flow-through subnetwork for X eventually dominates so that neither multiplicity nor oscillations can exist. Therefore the tip of the cusp points in the X_0 direction and the oscillatory region closes up.

(c) Basic features of any of the three bifurcation diagrams may be deduced from the other two. In particular, the anti-diagonal structure and the direction into which the cusp opens in Figure 1c is implied by Figure 1a,b; the curve connecting the cusp points in the $X_0-Z_0-k_0$ space must pass below the k_0-X_0 plane shown in Figure 1a and for higher values of X_0 than the reference BT point. Also, parts a and c of Figure 1

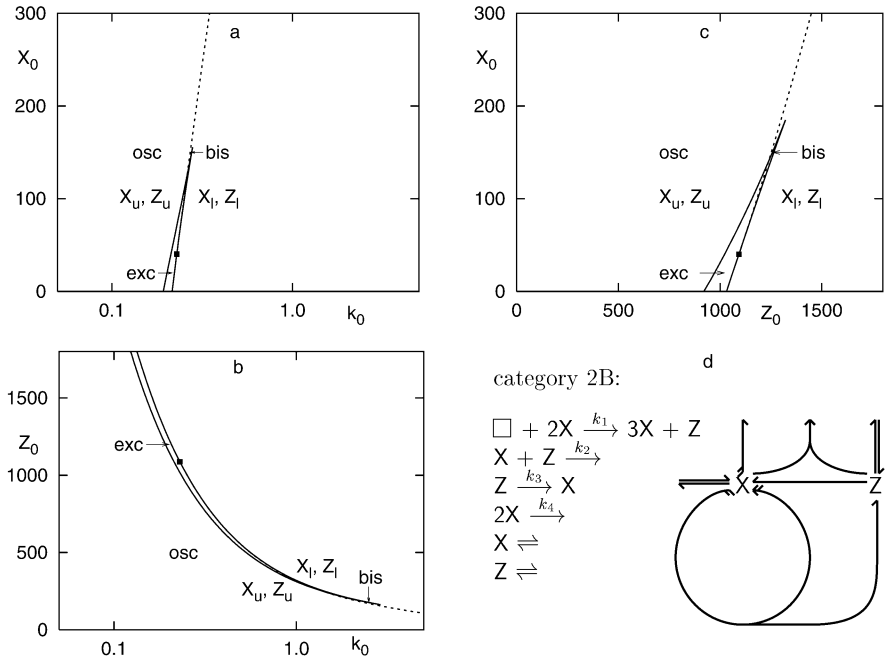

Figure 2. Bifurcation diagrams and reaction network for a prototype of category 2B. Rate coefficients used in calculations: $k_1 = 0.22404$, $k_2 = 0.11443$, $k_3 = 1.42369$, $k_4 = 0.017676$. Notation: solid line, saddle-node bifurcation; dashed line, Hopf bifurcation; square, BT point; osc, bis, exc, regions of oscillations, bistable stationary states, and excitability, respectively. Fixed parameter values for the reference BT point: $k_0 = 0.23$, $X_0 = 40.0$, $Z_0 = 1093$.

suggest that the crossover of the Hopf and saddle-node bifurcation curves not found in Figure 1b would occur if the diagram were generated for a smaller fixed value of X_0. (There must be such a crossover based on generic arguments.)

(d) The oscillatory region enclosed by the Hopf curve and the SNIPER bifurcation never extends to zero values of k_0 because oscillations in category 2C depend crucially on the inflow of *Z*. Also, the oscillatory region is highly asymmetric with respect to the cusp; it extends where the stationary state is "high" with respect to X. The k_0-X_0 diagram may sometimes have a bounded region of multiplicity terminated by two cusps. If so, then only the left one is associated with the Hopf curve and thus of primary interest within the context of categorization of oscillatory mechanisms.

2.2.2. Category 2B. This prototype has been derived[9] from a model of glycolysis.[21] Here we present a modified version (Figure 2d) that emphasizes the basic feature of a B category, namely that it can provide oscillations in a batch reactor (of course, it is assumed that some reactants, not shown in the network diagram, must be provided in surplus or buffered so that their concentrations are effectively constant and included in the rate coefficients). The mechanism in Figure 2d follows from a prototype of 1B category (a skeleton BZ reaction) by merging type Z and Y species into a single species that becomes type Z and assuming a second-order autocatalytic step with respect to X. Therefore, there is a strong current cycle as required for category 2 oscillators and, as a special feature, an exit reaction between X and Z that is necessary for oscillations when Z is recovered by a tangent rather than flow feedback. As in 2C, there are two essential species X and Z and three external constraints X_0, Z_0, and k_0.

The bifurcation diagrams in Figure 2 are distinctly different from those for the 2C category. The k_0-X_0 (Figure 2a) and Z_0-X_0 (Figure 2c) diagrams are diagonal unlike in 2C. The k_0-Z_0 (Figure 2c) diagram is anti-diagonal with the cusp pointing right-down as in 2C. The stationary state pattern is different: (X_u, Z_u) at the low flow rate side of the cusp and (X_l, Z_l) on the other side. The oscillatory region is asymmetric as in 2C but extends to zero flow rate and zero inflow concentrations implying batch oscillations as expected. The Hopf curve does not curve around the tip of the cusp and the oscillatory region does not enclose the cusp, which implies that the bistable region is near the tip unlike in 2C.

2.2.3. Categories 1CX and 1CW. There are three essential species, X, Y, and Z, in 1CX, Figure 3g, and an additional essential species, W, in 1CW, Figure 4g. The difference between these two categories is rather subtle: 1CX requires an inflow of type X species whereas 1CW does not; rather, an internal production of X from Y is involved. Generally, in a 1C category the exit reaction may produce W species that subsequently react with Y, or W may arise by a branching off the autocatalytic cycle (a tangent reaction), or may not appear at all. Bifurcation diagrams for all six combinations of X_0, Y_0, Z_0, and k_0 for a prototype of the 1CX category (modified Franck model[22]) are shown in Figure 3a−f. The Z_0-X_0 plot, Figure 3d, is analogous to that for 2C (Figure 1c), but the k_0-X_0 (Figure 3a) and k_0-Z_0 (Figure 3c) plots are diagonal unlike the corresponding diagrams for 2C. For the Hopf curve in Figure 3b,c to form a loop constituting the cross-shaped diagram, the removal of X needs to be of first order and an additional removal of Y via a first-order reaction has to be taken into account. The absence of the latter causes the oscillatory region to extend to zero values of the flow rate but the period of oscillations tends to infinity. In experimental systems falling into the 1CX category, such as the mixed Landolt system,[16,17] this feature is not observed and therefore we modified the prototype by adding the (slow) removal of Y. The oscillatory region in Figure 3a extends to zero values of X_0, which seems to contradict the requirement for a 1CX oscillator to have an inflow of X. However, the oscillations vanish at $X_0 = 0$ with an infinite period. (Remark: Two of the three BT points in Figure 3a are mutually connected by a Hopf bifurcation curve nearly coinciding with the saddle-node curve.)

Bifurcation diagrams for a prototype of the 1CW category

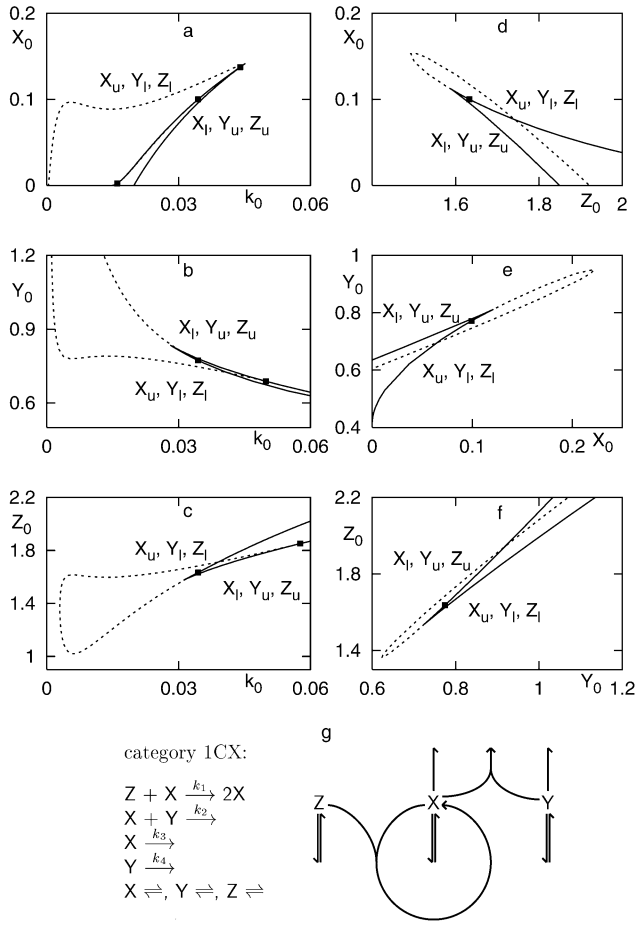

Figure 3. Bifurcation diagrams and reaction network for a prototype of category 1CX. Rate coefficients used in calculations: $k_1 = 0.31651$, $k_2 = 2.43584$, $k_3 = 0.07292$, $k_4 = 0.05$. Notation: solid line, saddle-node bifurcation; dashed line, Hopf bifurcation; square, BT point. Fixed parameter values for the reference BT point: $k_0 = 0.034$, $X_0 = 0.1$, $Y_0 = 0.77$, $Z_0 = 1.63$.

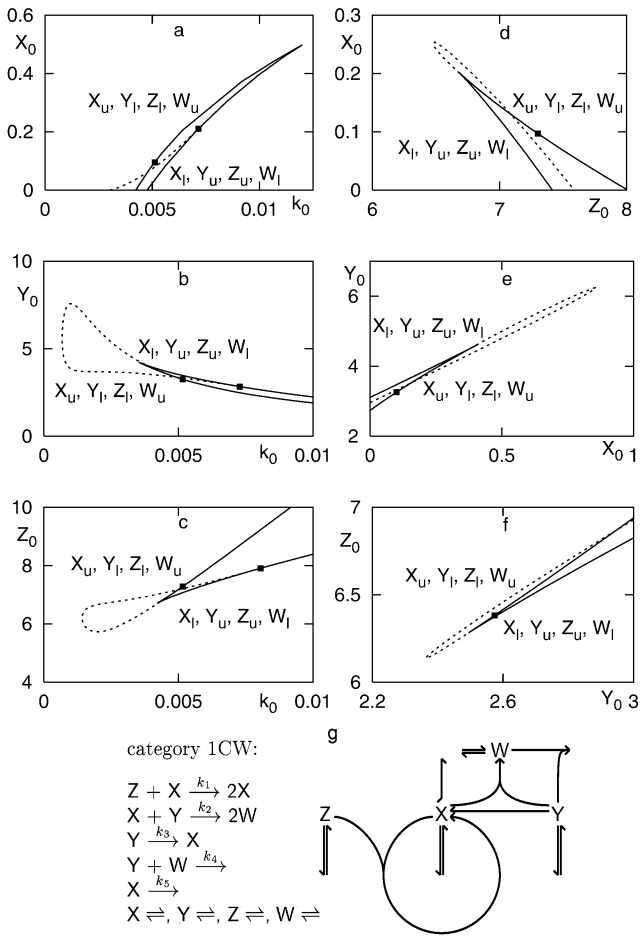

Figure 4. Bifurcation diagrams and reaction network for a prototype of category 1CW. Rate coefficients used in calculations: $k_1 = 0.0083786$, $k_2 = 0.73261$, $k_3 = 0.025$, $k_4 = 1.46522$, $k_5 = 0.02$. Notation: solid line, saddle-node bifurcation; dashed line, Hopf bifurcation; square, BT point. Fixed parameter values for the reference BT point: $k_0 = 0.0052$, $X_0 = 0.1$, $Y_0 = 3.3$, $Z_0 = 7.3$, $W_0 = 0.1$.

(essentially the minimal bromate oscillator[23]) are shown in Figure 4a−f for the same pairs of constraints as in Figure 3. Behavior of type W species, as indicated by the shift experiments, is identical to that of type X species.[1] Also, the bifurcation diagrams show the same kind of structure when plotting either X_0 or W_0 against any other constraint; therefore we have omitted type W species in the figure. There is virtually no difference in the corresponding diagrams for 1CX and 1CW. The extent of oscillatory regions may vary substantially when rate coefficients are changed. In some cases the Hopf bifurcation curve does not form a loop around the cusp; rather, it is contained within the cusp region and oscillatory regions disappear. Even so, the orientation of the cusp structure remains unchanged.

As in category 2, the structure of diagrams in a plane of two inflow concentrations can be deduced from the flow rate−inflow concentration diagrams.

2.2.4. Category 1B. This category has three essential species X, Y, and Z and hence four external constraints X_0, Y_0, Z_0, and k_0. The prototype, Figure 5g, is essentially the three-variable Oregonator.[24] The six corresponding bifurcation diagrams are shown in Figure 5, parts a−f. There is more correspondence between comparable diagrams for 2B and 1B categories than with the C categories. In particular, the flow rate−inflow concentration plots are consistent for 2B and 1B: diagonal for X_0, Figures 2a and 5a, and anti-diagonal for Z_0, Figures 2b and 5c. The diagrams for 1B show a region of multiplicity limited by two cusps, rather than one. This is due to a particular choice of rate coefficients; the left cusp in Figure 5a can be shifted to negative values of X_0. As expected for a B category, the oscillatory region extends to zero flow rates. The k_0-Y_0 and k_0-Z_0 diagrams in Figure 5b,c are identical up to a scaling factor and therefore the corresponding Y_0-Z_0 diagram in Figure 5f is peculiar in that the bifurcation lines are degenerate. All of them are parallel straight lines: there are two saddle-node bifurcation lines very close to each other, and a Hopf bifurcation line; eigenvalues along each line are constant. This is due to a special way the species Z and Y are linked in the network as mentioned already in Eiswirth et al.[1]

Generally, there may be more essential species of the same type in an experimental oscillator or in its realistic model, for example, more than one autocatalytic species is typically expected to form an autocatalytic loop. Corresponding bifurcation diagrams for the species of the same type will possess the same features and thus the process of determination of the category is reduced to that for the prototypes.

3. Relations between Bifurcation Diagrams and Concentration Shift Matrix

3.1. Local and Global Concentration Shift Matrix. In a flow-through reactor experiments may be carried out such that,

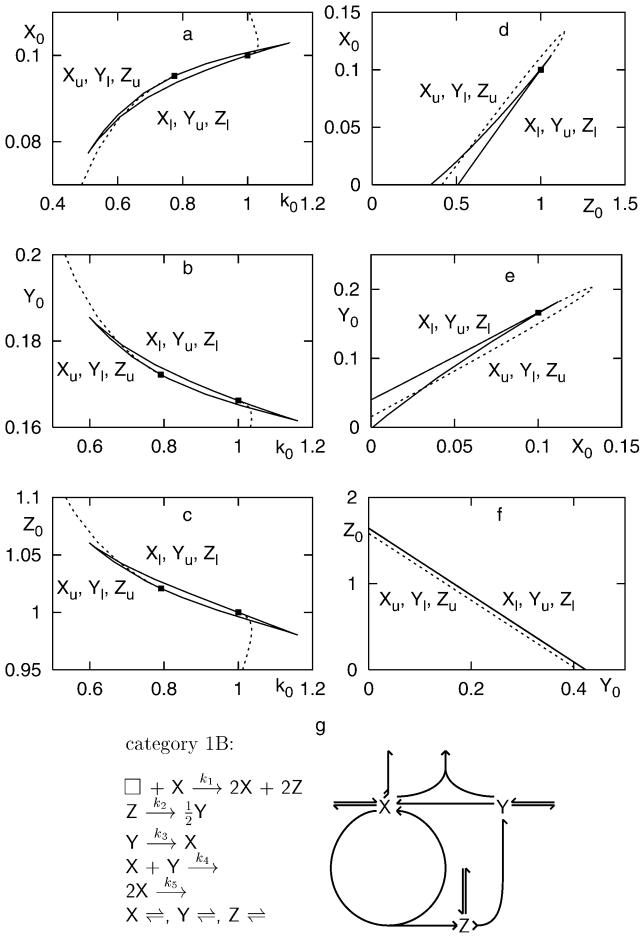

Figure 5. Bifurcation diagrams and reaction network for a prototype of category 1B. Rate coefficients used in calculations: $k_1 = 6.69803$, $k_2 = 1.06601$, $k_3 = 0.395$, $k_4 = 63.03$, $k_5 = 3.95$. Notation: solid line, saddle-node bifurcation; dashed line, Hopf bifurcation; square, BT point. Fixed parameter values for the reference BT point: $k_0 = 1.0$, $X_0 = 0.1$, $Y_0 = 0.166$, $Z_0 = 1.0$.

at a stable stationary state near a Hopf bifurcation, the inflow concentrations of the essential species are slightly increased one at a time and the observed change in the stationary state concentration of each species is measured. The resulting concentration shift matrix can be used as a tool for category determination and classification of essential species. When comparing experiments to a proposed mechanism, the concentration shift matrix may be readily calculated as the negative inverse of the Jacobian[3] (see eqs B2 and B3) and compared to experiments; only sign symbolic representation is necessary for determining the category. The elements of the shift matrix are measuring the sensitivity of stationary concentrations to changes in inflow concentrations. Since the flow rate is frequently used as a variable constraint, it is convenient to extend the matrix by one column expressing the sensitivity to the flow rate; see Appendix B for the derivations.

In general, the shift method is local by virtue of perturbing the stationary state only slightly (or infinitesimally in calculations). On the other hand, bifurcation diagrams may be viewed as a global extension of the shift experiments. Instead of a particular point in the space of constraints we are now considering the whole region probed by taking two-parameter slices. To see the effects of changing the constraints on the stationary state, concentrations of the species need to be measured when constructing the bifurcation diagram. To visualize the changes in concentration for a particular species in the prototypes of categories we take the reaction rate coefficients at the BT point used in generating the bifurcation diagrams and allow only one constraint to vary at a time while monitoring the stationary state concentrations of all species. The slopes of the curves in such a plot for each species at a given value of the constraint are simply the values from a corresponding column of the shift matrix. As an example, we show the flow rate−stationary-state-concentration diagrams for all the categories in Figure 6a−d. Each curve has three branches, two of them corresponding to an "upper" and a "lower" stationary state, and the third one in the middle corresponding to the saddle.

An important observation is that the curves are monotonic on the three respective branches when sufficiently close to the region of multiplicity. Consequently in this region all the elements of the concentration shift matrix determined locally at any value of the constraints have unique signs. In prototypes, this rule is mostly valid in a broad range of constraints and represents a typical behavior used for categorization. However, extremes on the curves may occur and the monotonicity holds no longer (for example, see lower branch for Z in Figure 6b). This restricts the range of constraints where the categorization based on local concentration shifts may be applied. Therefore the local concentration shift method for categorization is limited to the proximity of either a saddle-node bifurcation or a Hopf bifurcation[1] provided that the latter is not too far from the saddle-node bifurcation.

When two branches of stationary states overlap we can always uniquely assign one of them as upper and the other as lower with respect to each of the species. Thus the limitation of the local concentration shift method can be overcome if we consider the bifurcation diagrams Figures 1−5 and add the information on upper and lower stationary values for each species provided by diagrams in Figure 6. Now we can make the main conclusion of this section: whenever there is a *transition from an upper state to a lower state* as a chosen constraint is increased, the concentration shift regulation is *inverse* or *negative* (a minus sign in the symbolic shift matrix) and, conversely, a *transition from a lower state to an upper state* is associated with a *direct* or *positive* regulation (a plus sign in the symbolic shift matrix). Hence the sign-symbolic matrix of local concentration shifts can be replaced by a sign-symbolic matrix of global concentration shifts, which is easily derived from Figures 1−5 for each category considering the upper/lower transitions for each species in the direction of each constraint. In fact, flow rate−inflow concentration diagrams alone are sufficient for deriving the global concentration shift matrix, including the shifts with respect to k_0.

We denote an element of the (sign-symbolic) global shift matrix as Δ_{ij}, where i represents the ith species at stationary state and j represents the jth constraint (either the inflow concentration of a species or the flow rate). The global shift matrices for essential species in each category are shown in Table 1. By comparing the tilt of the cusp regions in the bifurcation diagrams and by the way the matrix was constructed we can make the following observations. (a) Columns: (1) each pair of columns must have either the same signs or exactly opposite signs of corresponding elements; (2) if two columns are the same, then the bifurcation diagrams in the corresponding constraints have anti-diagonal structure of the cusp; (3) if two columns are opposite, then the bifurcation diagrams in the corresponding constraints have diagonal structure of the cusp; and (4) rules 2 and 3 imply that two bifurcation diagrams with a common constraint can be used to predict the tilt of the cusp in the complementary bifurcation diagram with the common constraint left out. (b) Rows: (1) by symmetry, each pair of

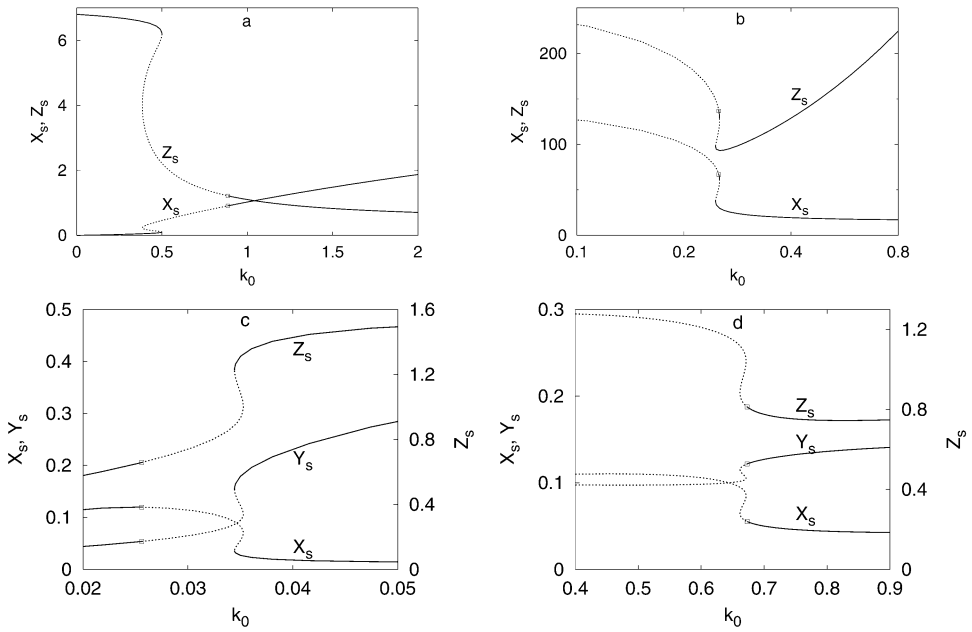

Figure 6. Dependence of stationary concentrations X_s, Y_s, and Z_s on flow rate for each category. (a) Category 2C: $X_0 = 0.5$, $Z_0 = 6.8$. (b) Category 2B: $X_0 = 100$, $Z_0 = 1000$. (c) Category 1CX: $X_0 = 0.1$, $Y_0 = 0.77$, $Z_0 = 1.63$. (d) Category 1B: $X_0 = 0.1$, $Y_0 = 0.18$, $Z_0 = 1.0$. Rate coefficients as in Figures 1, 2, 3, and 5, respectively. Notation: solid line, stable; dashed line, unstable; square, Hopf bifurcation.

TABLE 1: Global Sign-Symbolic Concentration Shift Matrix $\{\Delta_{ij}\}$ for Each Category

category 2C					category 2B				
i	*j*	X_0	Z_0	k_0	*i*	*j*	X_0	Z_0	k_0
X_s	Δ_{ij}	+	+	+	X_s	Δ_{ij}	+	−	−
Z_s		−	−	−	Z_s		+	−	−

category 1C						category 1B					
i	*j*	X_0	Y_0	Z_0	k_0	*i*	*j*	X_0	Y_0	Z_0	k_0
X_s		+	−	+	−	X_s		+	−	−	−
Y_s	Δ_{ij}	−	+	−	+	Y_s	Δ_{ij}	−	+	+	+
Z_s		−	+	−	+	Z_s		+	−	−	−

rows must follow rule 1 for columns; (2) when two rows are the same, the two species have the same regulation with respect to all constraints and are either of the same type, or else they are category specific—for 1B and 2B, X and Z have the same regulation, for 1C, Y and Z have the same regulation; and (3) two rows of opposite signs indicate mutually competitive action—in category 1, X and Y have always opposite regulation, for 1C and 2C, X and Z are opposite.

Thus by comparing regulation of two species S1 and S2 with respect to all constraints (i.e., two rows), we can infer the kind of reactions they are involved in. Opposite regulation suggests reaction of the type S1 + S2 → (as the exit reaction between X and Y in category 1, or the flow feedback reaction between X and Z in categories 1C and 2C); identical regulation suggests that the species S1 and S2 are produced by the same reaction (as X and Z in 1B or 2B) or both compete for the same species (as Y and Z in 1C). Implications of the rules for columns and rows will be fully explored in the following sections.

Because any two rows/columns are either the same or opposite, the minimal information necessary to construct the global shift matrix is to provide one row and one column, or one row/column and diagonal elements. To construct one row experimentally we need to measure the concentration of one species and vary all constraints; to construct one column we need to measure all species and vary one constraint. Although experimental construction of flow rate−inflow concentration bifurcation diagrams for all species requires only one species to be measured so as to indicate bistability and oscillations, such measurements provide only one row of the global shift matrix for the particular measured species. In Eiswirth et al.[1] another indicator, in addition to concentration shifts, was introduced. Namely, the stationary state at a Hopf bifurcation can be either stabilizing or destabilizing as the constraint is increased. Here again one species needs to be measured to determine whether oscillations change to a stationary state or vice versa, hence this method is equivalent to determining one row of the concentration shift matrix. In conclusion, to obtain the full matrix, all constraints must be varied and all species measured.

3.2. Effects of Including Nonessential Species into the Prototypes. The prototypes described in Section 2 involve by definition only essential species. We have shown that the bifurcation diagrams and the associated global shift matrix can be used to determine the connectivity of essential species in the (skeleton) reaction network. However, the bifurcation diagrams and the concentration shifts are defined equally well for both essential and nonessential species and so the rules outlined above in principle apply to any type of species. Therefore the bifurcation diagrams and the global shift matrix for a complete mechanism must provide some information on the connectivity of nonessential species. Since methods for distinguishing between essential and nonessential species are available,[1,3,4] we assume that nonessential species have already been identified and now we examine how their involvement in the network reflects itself in the bifurcation diagrams/concentration shift matrix.

First we take the 1CX category prototype and add three nonessential species of type a, b, and c, see Figure 7. In general, type a species is a *reactant* that produces an essential species by a first-order reversible reaction and is only weakly coupled to the network (the reaction Z → a is slow); type b species is a *product* weakly coupled to the network (b → X is slow); type c species is either a *reactant* that reacts with an essential species or an *intermediate* (as in Figure 7), possibly strongly coupled to the network which, if buffered, does not prevent the system from oscillations. As before with the essential species, we have constructed bifurcation diagrams in k_0-a_0, k_0-b_0, and k_0-c_0

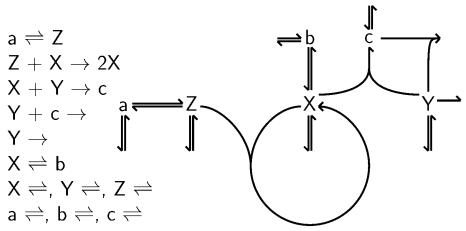

Figure 7. Reaction mechanism and network diagram for the 1CX category extended by adding nonessential species a, b, and c.

TABLE 2: Global Sign-Symbolic Concentration Shift Matrix $\{\Delta_{ij}\}$ for an Extended 1CX Category (1CX + a, b, c)

i	j	X_0	Y_0	Z_0	a_0	b_0	c_0	k_0
X_s		+	−	+	+	+	+	−
Y_s		−	+	−	−	−	−	+
Z_s	Δ_{ij}	−	+	−	−	−	−	+
a_s		−	+	−	−	−	−	+
b_s		+	−	+	+	+	+	−
c_s		+	−	+	+	+	+	−

parameter planes and determined the "lower" and "upper" stationary states. However, for the sake of brevity, we convert this information to the global shift matrix and use this representation only, see Table 2. We expect the submatrix for the essential species to provide clues for determining the connectivity among essential species. There are two alternatives, the flow feedback shown in Figure 7 with Z provided only in the feed, or an internal feedback with Z being produced by the exit reaction between X and Y. To determine which one is the actual case we need external information provided either by a method utilizing nonlinear dynamics, such as pulsed experiments,[3,25,26] or simply by knowledge of the underlying chemistry. Assuming that the actual subnetwork for essential species is as in Figure 7 we can proceed to the examination of the connectivity of nonessential species.

Type a species has the same row and column as the species Z to which it is coupled; likewise type b species has the same row/column regulation as the species X to which it is coupled. Hence a simple first-order reverse coupling to an essential species implies an identical regulation. Like type b, type c species has the same regulation as type X species, but we already know that c is an intermediate and hence cannot be simply coupled to X as b is. We can, for example, assume that its coupling to the network will be similar to the coupling of a type W species, that is, reaction X + Y → c is assumed. However, other couplings of c providing the same regulation are possible; for example, c could be produced from X without participation of *Y* and then react with Y. Therefore the global shift matrix provides alternatives rather than unique answers and further information is needed to decide which one is correct. As before, this information may be provided by pulsed experiments or by knowledge of the underlying chemistry.

The second example is the 1B category prototype extended by three type c nonessential species, see Figure 8. The species c1 and c2 enter the network as reactants by reacting with an essential species, and species c3 is an intermediate. The shift matrix is shown in Table 3; the submatrix corresponding to essential species is consistent with the 1B prototype. As with the 1C category, there are two possible ways species Z might be involved. One of them—possessing a *tangent feedback*—is the prototype itself. Here Z is produced by the tangent reaction c1 + X → 2X + 2Z and negative feedback is mediated by the reaction 2Z + c2 → Y. The other possible arrangement—displaying an *exit feedback*—produces Z by the exit reaction X + Y → Z and subsequently Z is converted to Y in the same

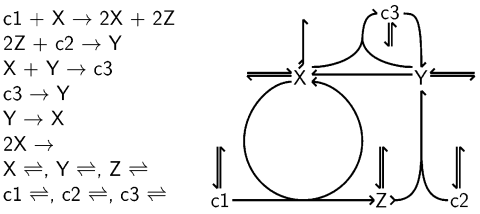

Figure 8. Reaction mechanism and network diagram for the 1B category extended by adding nonessential species c1, c2, and c3.

TABLE 3: Global Sign-Symbolic Concentration Shift Matrix $\{\Delta_{ij}\}$ for an Extended 1B Category (1B + c1, c2, c3)

i	j	X_0	Y_0	Z_0	$c1_0$	$c2_0$	$c3_0$	k_0
X_s		+	−	−	+	−	−	−
Y_s		−	+	+	−	+	+	+
Z_s	Δ_{ij}	+	−	−	+	−	−	−
$c1_s$		−	+	+	−	+	+	+
$c2_s$		−	+	+	−	+	+	+
$c3_s$		+	−	−	+	−	−	−

way as the species c3. As mentioned above, we need some auxiliary information to determine the actual connectivity of the essential species. Given that this information points to the tangent feedback as in Figure 8, the connectivity of nonessential species can be deduced as follows: the row in the shift matrix for c1 is opposite that for X and the column is the same as that for X. Moreover, c1 exhibits a negative self-regulation. Thus its shift behavior is the same as the shift behavior of the type Z species in the 1C category, which indicates that c1 reacts with X much like Z does in the 1C category. The species c2 has the same shift behavior as the type Y species and this suggests that c2 might react with X in an exit-like reaction; another possibility comes from observing that the row shift regulation of c2 is opposite not only to X but also to Z, which suggests that c2 might react with Z. Pulsed experiments or other external information is needed for correct determination. Finally, the species c3 shows the same regulation as Z and therefore should be involved in the exit feedback since Z itself is involved in the tangent feedback.

These examples suggest that the nonessential species should be identified before examining the shift matrix; the shift matrix cannot be used to distinguish various types of nonessential species (unlike the essential species). The shift regulation can be the same as that for an essential species, which together with the known type of species provides an important clue as to its involvement in the network. However, the shift regulation may not be consistent with any essential species within the given category. This itself is an indication that the species is nonessential but, more importantly, such a species may have shift behavior consistent with an essential species from another category (such as the Z-like regulation in 1C of the species c1 in the second example belonging to 1B) and that strongly suggests its connectivity.

In conclusion, the global shift matrix proves useful in the determination of connectivity in the network. It provides alternatives rather than unique choices for various parts of the network which, however, is still valuable input to the mechanism-determining procedure.

4. Determination of Reaction Mechanism from Bifurcation Diagrams

Belousov−Zhabotinsky Reaction. After examining prototypes of categories and their extension to include nonessential species for the purpose of calculating bifurcation diagrams we now focus on the reverse problem. For a more complex

TABLE 4: Reaction Mechanism and Rate Coefficients for a Modified FKN Mechanism of the BZ Reaction[a]

reaction no.	reaction	rate coefficient
(1)	$Br^- + HOBr + H^+ \rightarrow Br_2 + H_2O$	$k_1 = 8 \times 10^9\ M^{-2}\ s^{-1}$
(2)	$Br^- + HBrO_2 + H^+ \rightarrow 2HOBr$	$k_2 = 3 \times 10^6\ M^{-2}\ s^{-1}$
(3)	$Br^- + BrO_3^- + 2H^+ \rightarrow HOBr + HBrO_2$	$k_3 = 2\ M^{-3}\ s^{-1}$
(4)	$2HBrO_2 \rightarrow HOBr + BrO_3^- + H^+$	$k_4 = 3000\ M^{-1}\ s^{-1}$
(5, −5)	$HBrO_2 + BrO_3^- + H^+ \rightleftharpoons 2BrO_2^\bullet + H_2O$	$k_5 = 42\ M^{-2}\ s^{-1}$ $k_{-5} = 4.2 \times 10^7\ M^{-1}\ s^{-1}$
(6, −6)	$Ce^{3+} + BrO_2^\bullet + H^+ \rightleftharpoons Ce^{4+} + HBrO_2$	$k_6 = 8 \times 10^4\ M^{-2}\ s^{-1}$ $k_{-6} = 8.9 \times 10^3\ M^{-1}\ s^{-1}$
(7)	$Ce^{4+} + BrMA \rightarrow Ce^{3+} + Br^- + \text{products}$	$k_7 = 0.5\ M^{-1}\ s^{-1}$
(8)	$Br_2 + EnMA \rightarrow H^+ + Br^- + BrMA$	$k_8 = 6 \times 10^6\ M^{-1}\ s^{-1}$
(9,−9)	$H^+ + MA \rightleftharpoons EnMA + H^+$	$k_9 = 1.3 \times 10^{-2}\ M^{-1}\ s^{-1}$ $k_{-9} = 1.3 \times 10^4\ M^{-1}\ s^{-1}$

[a] MA ≡ $CH_2(COOH)_2$, EnMA ≡ $(OH)_2C{=}CHCOOH$, BrMA ≡ $BrCH(COOH)_2$.

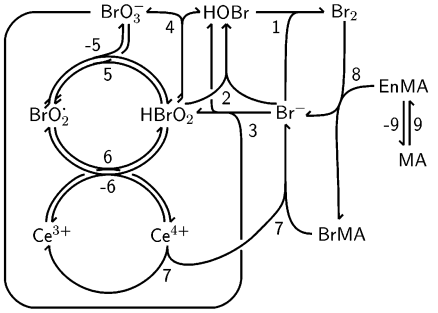

Figure 9. Network diagram for the FKN mechanism of the BZ reaction shown in Table 4. Species with effectively constant concentrations (H^+ and H_2O), inflows, and outflows are omitted.

mechanism,we calculate its bifurcation diagrams and then discuss the process of network reconstruction from those diagrams and the associated shift matrix. The reaction mechanism in Table 4 is a variant of the Field−Körös−Noyes model of the Belousov−Zhabotinsky reaction[14,15] with the organic part simplified according to Field and Noyes;[24] the rate constants are taken from Edelson et al.[15] and Field and Försterling.[27] The corresponding reaction network is shown in Figure 9. There are 11 species; some of them are very quickly reacting compounds or radicals which cannot be stored and fed into the reactor and therefore corresponding bifurcation diagrams are experimentally not feasible. For the sake of a complete picture, however, we calculate diagrams for every species and discuss the experimental feasibility later.

The nonessential species can be discerned by determining relative oscillatory amplitudes and quench vectors,[28] leaving $HBrO_2$, $BrO_2^\bullet$, Br^-, and Ce^{4+} as essential species. For a range of experimentally plausible constraints we calculated the inflow concentration−flow rate bifurcation diagrams for all species. The inflow concentrations for a reference point common to all bifurcation diagrams are the following: $[BrO_3^-] = 0.08$ M, $[MA] = 0.05$ M, $[Br^-] = 8.5 \times 10^{-4}$ M, $[Ce^{3+}] = 0.002$ M; inflow concentrations of other species are zero. The concentration of hydrogen ions in the reactor is assumed fixed, $[H^+] = 1.5$ M. For rate coefficients see Table 4. In addition, we calculated the dependence of stationary states on the flow rate k_0, which enables us to identify transitions between lower and upper stationary states. These results are shown in Figures 10−12. The two kinds of diagrams for each species form a pair and are grouped accordingly in the figures. We carry out as much of the analysis as possible by using Figures 10−12 and referring to bifurcation diagrams for prototypes. Then we reformulate the information in Figures 10−12 in terms of the global shift matrix and double-check the results.

The bifurcation diagrams for $HBrO_2$ and $BrO_2^\bullet$ are diagonal and display transitions from upper to lower stationary state as k_0 is increased (negative regulation with respect to k_0); this is consistent with type X species from 2B, 1B, or 1C. The bifurcation diagram for Br^- is anti-diagonal and the regulation with respect to k_0 is positive. Such behavior is consistent with type X species from 2C or with type Y species; the former is inconsistent with the assumed type X for $HBrO_2$ and $BrO_2^\bullet$. Thus we rule out category 2C and assume Br^- to be of type Y. Therefore category 2B is also ruled out but both 1B and 1C are still possible. The anti-diagonal bifurcation diagram for Ce^{4+} is consistent with type Z species in 1B and this is confirmed by a negative regulation with respect to k_0. (Remark: The two BT points in the $k_0-[Ce^{4+}]_0$ diagram in Figure 10 are connected by a Hopf bifurcation curve nearly coinciding with the saddle-node curve.) So far we can assume that $HBrO_2$ and $BrO_2^\bullet$ are involved in an autocatalytic cycle. An alternative is that one of them is a type W species that would be produced by an exit reaction $X + Y \rightarrow$. However, a 1B mechanism including W has not been found as yet and, moreover, by taking an argument from chemistry, the reaction of Br^- with either of $HBrO_2$ and $BrO_2^\bullet$ to produce the other does not proceed. Next we need to determine whether Ce^{4+}, the type Z species, is involved in a tangent or exit feedback. By looking at the nonessential species Ce^{3+} (Figure 11) we find that the diagonal cusp region and positive regulation with respect to flow rate are consistent with type Z behavior in category 1C. This is the same situation as with c1 in the previous example of extended 1B prototype, that is, Ce^{3+} should react with a type X species. This strongly suggests that Ce^{3+} reacts with $BrO_2^\bullet$ to provide Ce^{4+}, which in turn implies a tangent feedback for Ce^{4+}.

The species in Figures 11 and 12 are all nonessential. It should be noted that all of them have some irregularities in the shape of the region of multiple stationary states: either there are additional humps or there is no cusp at all. These features may be taken as indications of the nonessential nature of these species. As shown earlier, such irregularities do not need to occur in diagrams for nonessential species but may provide an independent confirmation.

BrO_3^- shows the same Z-like behavior as Ce^{3+} and therefore it should react with a type X species. The obvious choice is $HBrO_2$. HOBr has a diagonal cusp and positive regulation with respect to k_0. This is characteristic of the type X or W species; in fact, HOBr should be seen as W-like, since by being nonessential it cannot be a part of the autocatalytic cycle. This situation is analogous to that for the species c in the extended 1C prototype; therefore we deduce that HOBr is produced by the exit reaction $HBrO_2 + Br^- \rightarrow$. The bifurcation diagram for Br_2 is anti-diagonal and the regulation with respect to k_0 is negative, which is consistent with Z-like behavior (in 1B). This means that Br_2 is involved in either a tangent or exit negative feedback loop. Since the (primary) tangent feedback is already

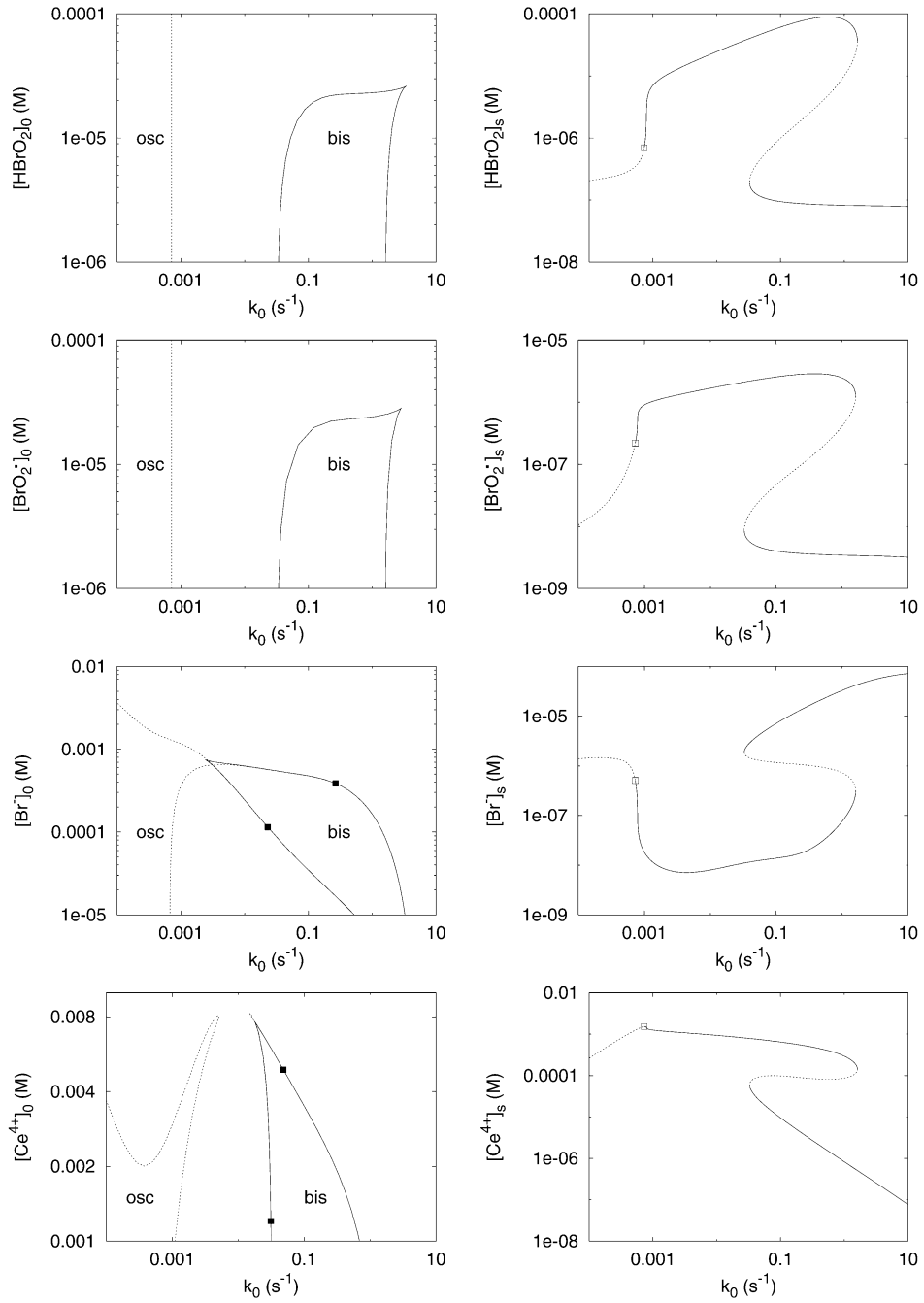

Figure 10. Bifurcation diagrams (left) and corresponding stationary state diagrams (right) of essential species for the FKN model. Notation in bifurcation diagrams: solid line, saddle-node bifurcation; dashed line, Hopf bifurcation; solid square, Bogdanov-Takens point; osc, bis, region of oscillations and bistable stationary states, respectively. Notation in stationary state diagrams: solid line, stable; dashed line, unstable; open square, Hopf bifurcation point. For parameter values see Table 4 and text.

associated with (the essential species) Ce^{4+} we should formulate a reaction that would mediate an (secondary) exit feedback. This can be done by assuming that HOBr formed by the exit reaction gives rise to Br_2, which in turn should react to form Br^- so that the negative feedback is accomplished. By chemistry arguments the first of the two reactions should combine HOBr and Br^-.

By the same arguments, the other reaction, reduction of Br_2 to Br^-, is expected to involve bromination of malonic acid MA or its enol form EnMA. We can verify this hypothesis against bifurcation and regulatory behavior of EnMA and MA. Indeed, regulation of both EnMA and MA is opposite that for Br_2, suggesting that Br_2 reacts with EnMA or MA. Bifurcation diagrams for both EnMA and MA are without cusp and can be assigned neither diagonal nor anti-diagonal structure. These two species have the same (and rather degenerate) behavior signifying that they are mutually coupled by a reverse reaction. This situation is similar to the pairs of species a and Z or b and X in the extended prototype of the 1C category in Figure 7. However, which of the species EnMA and MA is reacting with Br_2 cannot be deduced from these diagrams. The bromination of EnMA (or MA) produces Br^- (completing thereby the exit feedback) and bromomalonic acid, BrMA.

Finally, two diagrams for BrMA are somewhat difficult to interpret. The cusp region is distorted and bent near the tip; nevertheless, we classify it as a slightly distorted anti-diagonal rather than a strongly distorted diagonal structure. The regulation is negative with respect to k_0 and both diagrams combined imply negative self-regulation for BrMA. This regulation clearly points

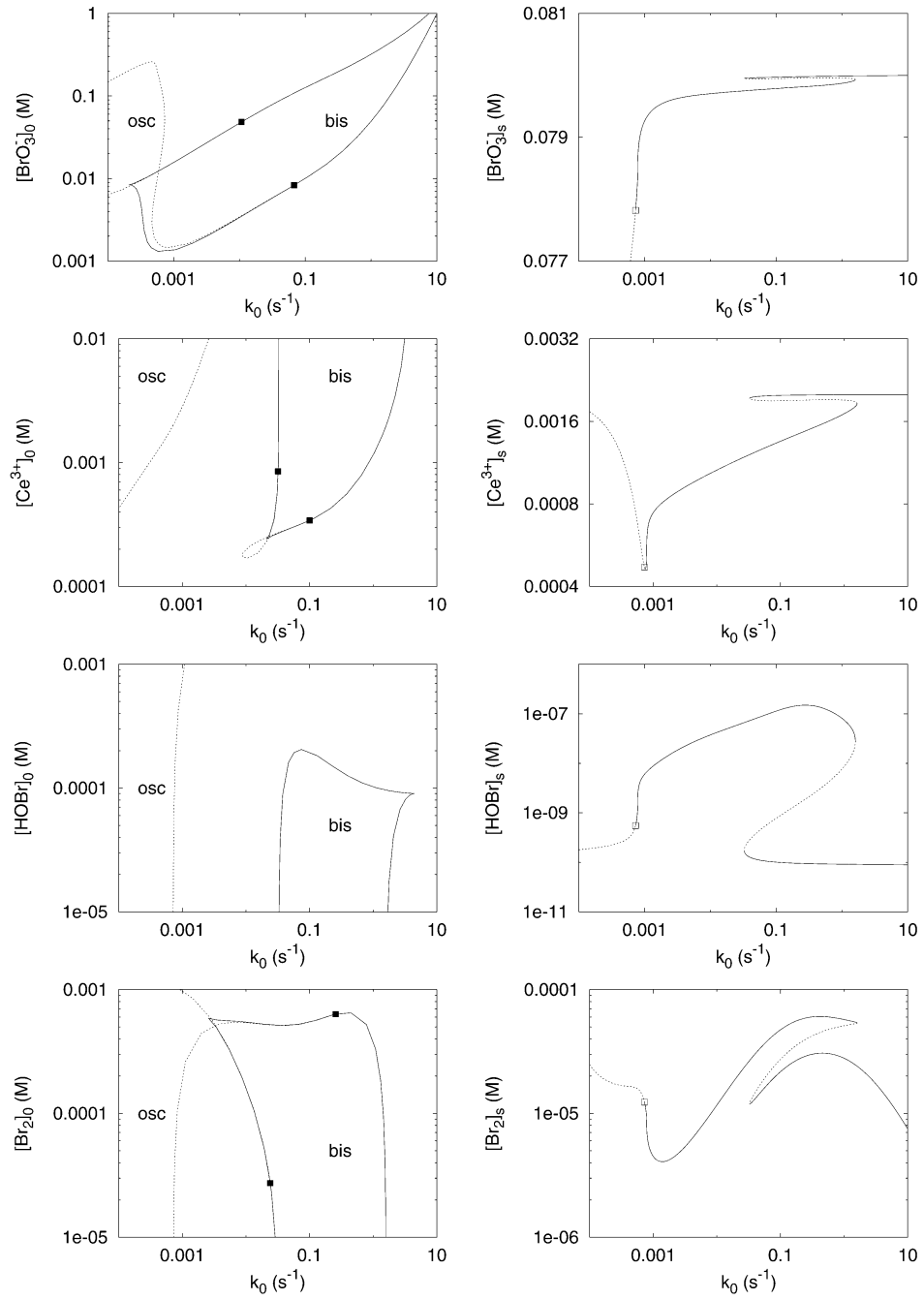

Figure 11. Bifurcation diagrams (left) and corresponding stationary state diagrams (right) of inorganic nonessential species for the FKN model. Notation and parameters as in Figure 10.

to Z-like behavior and is consistent with the assumed anti-diagonal bifurcation diagram. These observations suggest that BrMA feeds back to Br^-; however, the same regulation with respect to k_0 as Ce^{4+} seems to rule out a mutual reaction in contrast to the actual case.

As an alternative to the use of bifurcation diagrams one can derive from Figures 10−12 the global shift matrix, shown in Table 5. By inspecting this table we can deduce and confirm the same features of the network connectivity. In particular, the key features are derived from the *Z*-like behavior of the nonessential species BrO_3^-, Ce^{3+} (as in 1C), and Br_2 and BrMA (as in 1B) indicated by negative diagonal elements and by comparing the corresponding rows with the prototypes.

As a result, we were able to deduce reactions 1, 2, 5, 6, 8, and 9 and partly deduce reaction 7; reactions 3 and 4 are masked by shift behavior characteristic of other reactions. Whether the reactions are reversible or nearly irreversible cannot be stated.

5. Discussion and Conclusions

Bifurcation diagrams in external constraints calculated for a prototype of each category of oscillatory reactions suggest that specific features in the reaction network of an examined oscillatory reaction can be identified by specific patterns in the corresponding diagrams. As already pointed out in Eiswirth et al.[1] the decisive feature is the tilt of the cusp-shaped region of multiple stationary states. Supplementary clues are provided by the location of oscillatory or excitable regions adjacent to the region of bistability. It is sufficient to construct the inflow concentration−flow rate diagrams for every species; the tilt in the inflow concentration−inflow concentration diagram for any

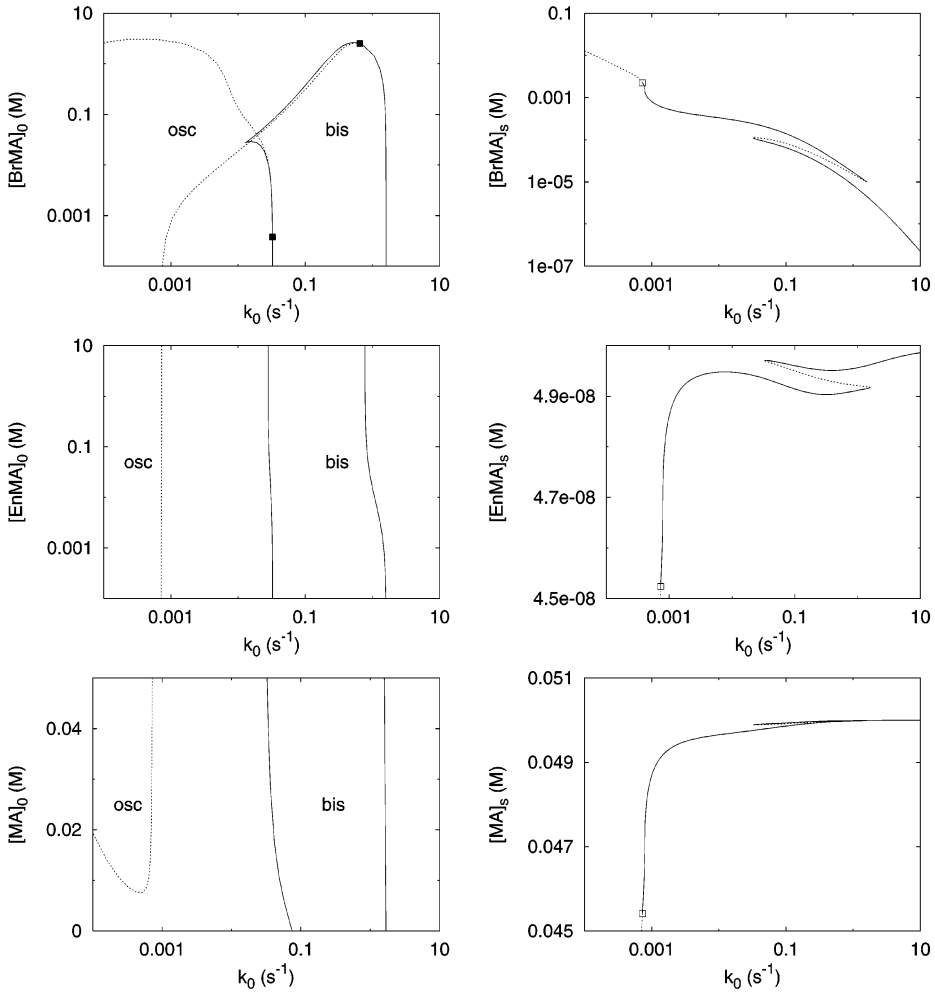

Figure 12. Bifurcation diagrams (left) and corresponding stationary state diagrams (right) of organic nonessential sqpecies for the FKN model. Notation and parameters as in Figure 10.

TABLE 5: Global Sign-Symbolic Concentration Shift Matrix $\{\Delta_{ij}\}$ for the FKN Mechanism of the BZ Reaction

		essential species				nonessential species							
i	j	$[HBrO_2]_0$	$[BrO_2^\bullet]_0$	$[Br^-]_0$	$[Ce^{4+}]_0$	$[BrO_3^-]_0$	$[Ce^{3+}]_0$	$[HOBr]_0$	$[Br_2]_0$	$[BrMA]_0$	$[EnMA]_0$	$[MA]_0$	k_0
$[HBrO_2]_s$		+	+	−	−	+	+	+	−	−	?	?	−
$[BrO_2^\bullet]_s$	Δ_{ij}	+	+	−	−	+	+	+	−	−	?	?	−
$[Br^-]_s$		−	−	+	+	−	−	−	+	+	?	?	+
$[Ce^{4+}]_s$		+	+	−	−	+	+	+	−	−	?	?	−
$[BrO_3^-]_s$		−	−	+	+	−	−	−	+	+	?	?	+
$[Ce^{3+}]_s$		−	−	+	+	−	−	−	+	+	?	?	+
$[HOBr]_s$		+	+	−	−	+	+	+	−	−	?	?	−
$[Br_2]_s$	Δ_{ij}	+	+	−	−	+	+	+	−	−	?	?	−
$[BrMA]_s$		+	+	−	−	+	+	+	−	−	?	?	−
$[EnMA]_s$		−	−	+	+	−	−	−	+	+	?	?	+
$[MA]_s$		−	−	+	+	−	−	−	+	+	?	?	+

pair of species is implied (see rule 4 for columns in Section 3.2). If the information about "lower" and "upper" stationary states is added, the bifurcation diagram becomes a powerful tool not only for distinguishing among categories and for determination of essential species, but also for reconstruction of reaction networks. In particular, transitions between "lower" and "upper" stationary states across the boundary of the cusp in the bifurcation diagrams can be arranged into a global concentration shift matrix, which is intimately connected with a (local) concentration shift matrix formulated as a tool for mechanism determination in prior work.[1,3,7] These matrices are written in a sign symbolic form; by comparing columns/rows for pairs of various species the mechanism can be at least partially reconstructed.

In the case of the FKN mechanism for the BZ reaction we were able to reconstruct most of the reaction network provided that all reacting species can be measured and all these species can also be added in the feed. While the first part of the assumption may be experimentally feasible, the second part may not be, because highly reactive intermediates cannot be fed continuously into the reactor. The question arises how far the reconstruction of the network connectivity can be carried out in such a case. The reactive intermediates are $HBrO_2$, $BrO_2^\bullet$, HOBr, and EnMA. Thus the corresponding bifurcation diagrams in Figures 10−12 are not available and likewise the corresponding columns in the global shift matrix in Table 5 are left out. On the basis of measurements of relative oscillatory amplitudes we can still discern essential and nonessential species. Thus Br^-

and Ce^{4+} can be safely determined as type Y and Z species, respectively. Since Ce^{4+} has a negative regulation with respect to flow rate, the category must be 1B. $HBrO_2$ and $BrO_2^{\bullet}$ have the same negative regulation with respect to flow rate as Ce^{4+} (and hence the same rows in the shift matrix); so they may be of type Z or type X. The missing clue can be provided by another method for classification, namely by oscillatory phase shifts:[3,9] type Z species in 1B are phase delayed with respect to type X species. This information is accessible since we assume that all species can be measured. Further reasoning about the network connectivity can rely on the same arguments as discussed in Section 4 up to the point of determining HOBr. The missing bifurcation diagram (or column in the shift matrix) leaves undecided whether this species should be seen as W-like or Z-like. Again, this can be decided from the phase shift of oscillations: W-like behavior should be in phase with type X species, Z-like behavior should be in phase with type Z species and delayed with respect to type X species. Finally, the bifurcation diagrams for EnMA and MA are degenerate (and the corresponding columns are undetermined); therefore implications are equally incomplete whether EnMA can be fed in or not. Thus the FKN network can be reconstructed to the same extent.

We have shown that the task of reconstructing reaction networks from measurements based on methods of nonlinear dynamics and bifurcations can be followed to a great extent by using bifurcation diagrams and transitions between "lower" and "upper" stationary states. If combined with other methods for classification and determination of oscillatory reaction mechanisms this approach enables us to reconstruct the network—or at least an essential part of it—even if limitations in feeding unstable intermediates into the reactor are taken into account. Thus the whole set of methods systematically studied in this and earlier papers[1,3−9,25,26,29] provides a useful systematic tool that can be used in cases where the classical intuition-based approach does not give satisfactory results, or can be used to help decide between alternative proposed mechanisms.

6. Appendices

Appendix A: Basic Notions from the SNA Theory.[2] Assume that there are m species taking part in r chemical reactions so that n species, $n \geq m$, are entering at least one of the reactions

$$\mathrm{R}_j: \qquad \sum_{i=1}^{n} \nu_{ij}^{\mathrm{L}} \mathrm{X}_i \rightarrow \sum_{i=1}^{m} \nu_{ij}^{\mathrm{R}} \mathrm{X}_i, \quad j = 1, \cdots, r \qquad \text{(A1)}$$

where ν_{ij}^{L} and ν_{ij}^{R} are respectively the left-hand and right-hand stoichiometric coefficients of species X_i in reaction R_j. The *first* n species are reactants or intermediates and the remaining $m - n$ are products. Let $\bar{\nu} = \{\nu_{ij}^{\mathrm{R}} - \nu_{ij}^{\mathrm{L}}\}$ be the $(n \times r)$ stoichiometric matrix, $x = (x_1, \cdots, x_n)$ the vector of the chemical species concentrations, and $\bar{v}(x) = (v_1(x), \cdots, v_r(x))$ the vector of reaction rates. The chemical equations A1 together with the vector function $\bar{v}(x)$ define the mechanism of the reaction, also called a stoichiometric network. Only the concentrations of reactants and intermediates are dynamical variables for which independent dynamical equations can be written. The time evolution of x in a flow-through system at constant temperature in a well-stirred reaction cell of constant reaction volume is

$$\frac{\mathrm{d}x}{\mathrm{d}t} = f(x) = \bar{\nu}\bar{v}(x) + k_0(x_0 - x) = \nu v(x) \qquad \text{(A2)}$$

where $x_0 = (x_{01}, \cdots, x_{0n})$ is the vector of feed concentrations for each species and k_0 is the flow rate (or more accurately, the reciprocal residence time). The inflow and outflow terms can be formally treated as zeroth- and first-order pseudoreactions, respectively, and can be included in an extended reaction rate vector $v(x) = (\bar{v}, k_0 x_0, k_0 x)$. Accordingly, by rewriting the flow term $k_0(x_0 - x)$ as $k_0 I(x_0 - x)$, where I is identity matrix, an extended stoichiometric matrix is $\nu = [\bar{\nu}, I, . -I]$. Thus the overall rate function $f(x)$ in (2) can be expressed in a compact form $f(x) = \nu v(x)$.

A stationary state x_s satisfies the equation $\nu v(x) = 0$. Hence $v_s = v(x_s)$ is contained in the null space of ν. Moreover, all components of v must be nonnegative numbers, which narrows the set of all possible stationary reaction rate vectors v_s (the currents in SNA terminology) to an open, convex, d_r-dimensional cone, $d_r = r - rank(\nu)$, in the space of all v's. The edges of this stationary state cone represent sets of stationary states that have minimum possible nonzero v_j's admitted by (2), and uniquely define a set of major subnetworks (or extreme currents) of the mechanism. In general, the number K of such subnetworks equals at least the dimension of the cone, $K \geq d_r$. Denote by e_k, $k = 1, ..., K$ the (arbitrarily normalized) vectors pointing along the edges of the cone. Any linear combination $\sum_{k=1}^{K} \alpha_k e_k$ with nonnegative coefficients is again a current. Conversely, any current v_s can be expressed as a linear combination of extreme currents (such a decomposition is, however, not unique if $K > d_r$). If the e_k's are suitably normalized, for example so that $\sum_{j=1}^{r} e_{kj} = 1$, $k = 1, ..., K$, then the numbers $\bar{\alpha}_k = \alpha_k / \sum_{k=1}^{K} \alpha_k$ quantify the contribution of extreme currents to a particular current. Certain subsets of extreme currents span subcones that are d-dimensional faces of the stationary state cone, $d = 2, ..., d_r - 1$. Hence there is a hierarchy of subnetworks associated with edges and faces of the stationary state cone that may be used as simplified models instead of the full network.

The identification of the edges and faces is useful when examining the stability of the (sub)network at a stationary state x_s. The Jacobian J of eq A2 at x_s is

$$J = \frac{\mathrm{d}f}{\mathrm{d}x}\Big|_{x=x_s} = \nu \frac{\mathrm{d}v}{\mathrm{d}x}^{x=x_s} = \nu(\mathrm{diag}\ v_s)\kappa^T (\mathrm{diag}\ x_s)^{-1} \qquad \text{(A3)}$$

where $v_s = \sum_{k=1}^{K} \alpha_k e_k$ and the kinetic matrix $\kappa = \{\kappa_{ij}\} = \{\partial \ln v_j(x_s)/\partial \ln x_i\}$.The number κ_{ij} is the effective order of the jth reaction with respect to the ith species; if the reaction rates obey power law then κ_{ij} is independent of x_s. Thus a reparametrization of the system (A2) is suggested such that $x_{s1}, ..., x_{sn}$ and $\alpha_1, ..., \alpha_K$ are new parameters.

If power law kinetics is in effect, the stability of the current v_s is indicated by principal subdeterminants β_l of order l, $l = 1, ..., n$ of the matrix

$$V = \nu(\mathrm{diag}\ v_s)\kappa^T \qquad \text{(A4)}$$

There are $\binom{n}{l}$ different β_l's related to all permutations of l species. If at least one of them is negative, then at least one eigenvalue of J is unstable provided that the values of the stationary state concentrations of the corresponding species are sufficiently small.[2] Since $v_s = \sum_{k=1}^{K} \alpha_k e_k$, the stability of the network's stationary states depends on the stability of the extreme subnetworks. An unstable e_k induces instability of the entire network if the corresponding α_k is large enough and x_s satisfies the requirement of small concentration of those species for which the corresponding $\beta_l < 0$. When linearly combined, the stable e_k's usually do not form an unstable current (then

they are called mixing stable), but an instability may occur, since $v(x)$ is generally nonlinear in x.

A network diagram is a convenient graphical representation of mass action networks. Any elementary reaction is drawn as a multiheaded multitailed arrow oriented from species entering the reaction to those produced by the reaction: the number of feathers (barbs) at each tail (head) represents the stoichiometric coefficient of the reactant (product); the order of the reaction is the number of left feathers. A graph theoretical approach allows for checking the stability of a (small enough) network by inspection of the graph.[2]

Appendix B: Classification/Categorization Approach.[1] Two classes of species are recognized, the *essential* and *nonessential* species, which are distinguished primarily by measuring their relative amplitudes of oscillations and their quench amplitudes. The nonessential species may be one of three types: type a species are reactants with a negligible feedback, type b species are products with a negligible feedback, and type c species are those intermediates which can be buffered without losing the oscillations. The nonessential species have either small relative amplitude (type a) or large quench vectors (type b) or both (type c); all types can be buffered without losing the oscillatory dynamics. The essential species have large oscillatory amplitudes and, if buffered, the oscillatory dynamics is lost; there are type X or *autocatalytic species* which occur on an autocatalytic cycle with positive feedback, type Y or *exit species* which react with type X species (by so-called exit reaction) thereby inhibiting the autocatalysis, and type Z or *feedback species* which take part in a negative feedback loop controlling the oscillations. In addition, in some cases there may be a type W or *recovery species* which is produced by an exit or tangent reaction. The experiments of type I, III, IV, and VI (as listed in the Introduction) are particularly useful for the classification of species.

There are two main categories distinguished by certain features of their reaction network: (a) category 1 involves an exit reaction (hence involving also type Y species) in addition to reactions of the autocatalytic cycle and the controlling negative feedback loop, and (b) category 2 does not have an exit reaction (and therefore no type Y species), instead, it possesses a higher order reaction on the autocatalytic cycle. This feature implies that category 2 oscillators encompass abstract or simplified schemes rather than detailed mechanisms consisting of elementary steps. Both main categories are further divided into subcategories, 1B, 1CX, 1CW and 2B, 2C, respectively. The role of essential species in each category is specific for that category and the corresponding classification is found in the process of determining the category. Experiments in (I), (II), and (VII) are the main tools for accomplishing this task.

In this paper a link between the sign-symbolic global/local concentration shift matrix and bifurcation diagrams has been established. It is interesting to note that at a stationary state near the Hopf bifurcation the local concentration shift matrix itself is linked to the Jacobian matrix and thus methods II, V, and VII for category and mechanism determinations are interlinked.

Assuming that the stationary state x_s of (2) depends on x_0 we can write

$$0 = f(x) = \bar{\nu}\bar{v}(x_s(x_0)) + k_0(x_0 - x_s(x_0)) \qquad \text{(B1)}$$

The local concentration shift matrix $\{\delta x_{si}/\delta x_{0j}\}$ is experimentally obtained by measuring a change δx_{si} in the ith stationary state concentration as a response to a change δx_{0j} in the jth inflow concentration. For small variations in constraints this matrix can be approximated[3] by (dx_s/dx_0), which is obtained from (5) upon differentiating with respect to x_0,

$$\frac{dx_s}{dx_0} = -k_0 J^{-1} \qquad \text{(B2)}$$

where $J = (df/dx)|_{x=x_s}$ is the Jacobian matrix. Here we assume that the stationary point is nondegenerate stable (near a Hopf bifurcation), and therefore J is invertible. Hence the local shift concentration matrix is proportional to the inverse of the Jacobian matrix. Similarly, upon differentiating (5) with respect to k_0 we obtain an additional column of the shift matrix expressing the sensitivity of the stationary state with respect to changes in k_0,

$$\frac{\partial x_s}{\partial k_0} = -J^{-1}(x_0 - x_s) \qquad \text{(B3)}$$

Acknowledgment. This work was supported in part by the National Science Foundation and by grant GA203/03/0488 from the Grant Agency of the Czech Republic.

References and Notes

(1) Eiswirth, M.; Freund, A.; Ross, J. *Adv. Chem. Phys.* **1991**, *80*, 127; *J. Phys. Chem.* **1991**, *95*, 1294.
(2) Clarke, B. L. *Adv. Chem. Phys.* **1980**, *43*, 1.
(3) Chevalier, T.; Schreiber, I.; Ross, J. *J. Phys. Chem.* **1993**, *97*, 6776.
(4) Stemwedel, J. D.; Schreiber, I.; Ross, J. *Adv. Chem. Phys.* **1995**, *89*, 327.
(5) Strasser, P.; Stemwedel, J. D.; Ross, J. *J. Phys. Chem.* **1993**, *97*, 2851.
(6) Stemwedel, J.; Ross, J. *J. Phys. Chem.* **1995**, *99*, 1988.
(7) Hung, Y.-F.; Ross, J. *J. Phys. Chem.* **1995**, *99*, 1974.
(8) Hung, Y.-F.; Schreiber, I.; Ross, J. *J. Phys. Chem.* **1995**, *99*, 1980.
(9) Schreiber, I.; Hung, Y.-F.; Ross, J. *J. Phys. Chem.* **1996**, *100*, 8556.
(10) Noszticius, Z.; McCormick, W. D.; Swinney, H. L. *J. Phys. Chem.* **1998**, *93*, 2796.
(11) Olsen, R. J.; Epstein, I. R. *J. Chem. Phys.* **1991**, *94*, 3083; *J. Chem. Phys.* **1993**, *98*, 2805.
(12) Ringland, J. *J. Chem. Phys.* **1991**, *95*, 555.
(13) De Kepper, P.; Pacault, A. *C. R. Seances Acad. Sci., Ser. C* **1978**, *286*, 437. De Kepper, P.; Boissonade, J. In *Oscillations and Traveling Waves in Chemical Systems*; Field, R. J., Burger, M., Eds.; Wiley: New York, 1985; . 223.
(14) Field, R. J.; Körös, E.; Noyes, R. M. *J. Am. Chem. Soc.* **1972**, *94*, 8649.
(15) Edelson, D.; Field, R. J.; Noyes, R. M. *Int. J. Chem. Kinet.* **1975**, *7*, 417.
(16) Gáspár, V.; Showalter, K. *J. Am. Chem. Soc.* **1987**, *109*, 4869.
(17) Edblom, E. C.; Györgyi, L.; Orbán M.; Epstein, I. R. *J. Am. Chem. Soc.* **1987**, *109*, 4876.
(18) Luo, Y.; Epstein, I. R. *J. Phys. Chem.* **1989**, *93*, 1398.
(19) Kubíček, M.; Marek, M. *Computational Methods in Bifurcation Theory and Dissipative Structures*; Springer: New York, 1983. Marek, M.; Schreiber, I. *Chaotic Behaviour of Deterministic Dissipative Systems*, Cambridge University Press: Cambridge, UK, 1995.
(20) Selkov, E. E. *Eur. J. Biochem.* **1968**, *4*, 79.
(21) Termonia, Y.; Ross, J. *Proc. Natl. Acad. Sci. U.S.A.* **1981**, *78*, 2952.
(22) Franck, U. F. In *Temporal Order*; Rensing, L., Jaeger, N. I., Eds.; Springer: Berlin, Germany, 1985; pp 2−12.
(23) Noyes, R. M.; Field, R. J.; Thompson, R. C. *J. Am. Chem. Soc.* **1971**, *93*, 7315.
(24) Field, R. J.; Noyes, R. M. *J. Chem. Phys.* **1974**, *60*, 1877.
(25) Vance, W; Arkin, A.; Ross, J. *PNAS* **2002**, *99*, 5816.
(26) Sanchez-Torralba, A.; Yu, K.; Shen, P.; Oefner, P. J.; Ross, J. *PNAS* **2003**, *100*, 1494.
(27) Field, R. J.; Försterling, H.-D. *J. Phys. Chem.* **1986**, *90*, 5400.
(28) Hynne, F.; Sørensen, P. G.; Nielsen, K. *J. Chem. Phys.* **1990**, *92*, 1747; *J. Chem. Phys.* **1990**, *92*, 4778.
(29) Arkin, A.; Ross, J. *J. Phys. Chem.* **1995**, *99*, 970.